Fully gapped type-II superconductivity in Pt-doped $IrTe_2$ near critical doping

Aastha Vasdev, Deepti Rana, Amit Vashist, Yogesh Singh, and Goutam Sheet*
Department of Physical Sciences, Indian Institute of Science Education and Research Mohali, Sector 81, S. A. S. Nagar, Manauli, PO 140306, India

(Received 4 January 2022; revised 9 February 2022; accepted 7 March 2022; published 21 March 2022)

The Dirac point in Pt-doped $IrTe_2$ is known to be tuned by controlling the doping concentration. For 10% Pt, it is seen that the Dirac point exists close to the Fermi energy of the system. This leads to the expectation that, for such doping, the system might host unconventional (topological) superconductivity. Here, we present a detailed microscopic and spectroscopic investigation of Pt-$IrTe_2$ under an ultrahigh vacuum, low-temperature scanning tunneling microscope. We find that, for the crystals of $Ir_{0.9}Pt_{0.1}Te_2$, the surface shows patches of atomic scale over which defects are seen to be randomly distributed. Tunneling spectroscopy reveals that $Ir_{0.9}Pt_{0.1}Te_2$ condenses into a fully gapped Bardeen-Cooper-Schrieffer-like (BCS) s-wave superconducting state. The superconducting gap was measured to be 460 μeV at 310 mK. The value of $2\Delta_0/k_BT_c \sim 6$ is consistent with a conventional BCS superconductor in the strong-coupling limit. The conventional behavior is surprising, given the topological band structure of the material.

DOI: 10.1103/PhysRevB.105.094509

I. INTRODUCTION

Among the chalcogenides, $IrTe_2$ is especially interesting from the structural point of view and for the presence of large spin-orbit coupling. Despite being a layered structure, the layers are bonded to each other by significant Te-Te interaction rather than weak van der Waals force [1]. The system shows a structural phase transition from a high-temperature trigonal to a low-temperature triclinic phase at around 270 K [2–5], where anomalies of resistivity and magnetic susceptibility were observed [6]. Several different mechanisms such as a charge or orbital density wave [7], an orbital-induced Peierls instability [8,9], crystal field of Te p orbital [3,10,11], the disappearance of a van Hove singularity close to the Fermi level [11], or an anionic depolymerization transition [12] were suggested to be the origin of the structural transition in $IrTe_2$. First-principles calculations showed that it was a consequence of the competition between Te-Ir, covalent/ionic, and Te-Te-covalent p-electron bonding [13]. However, it was also shown that the charge-transfer energy in $IrTe_2$ is close to zero and that the Te $5p$ states are also important for the low-energy physics by photoemission and optical studies [8,10,11].

Like many other two-dimensional (2D) materials, $IrTe_2$ has also been investigated in the context of superconductivity. The superconducting behavior of $IrTe_2$ is still a matter of debate. Initially, it was believed that pure $IrTe_2$ would not superconduct down to 0.32 K [14]. Recently, it was shown that pristine $IrTe_2$ superconducts below 2.5 K [10,15,16] where the superconductivity observed was thought to originate either at the surface or in filamentary form [17]. This was attributed to the Ir vacancies or excess Te in the samples [10,18]. It was also suggested that high carrier density might be required for the stabilization of superconductivity in $IrTe_2$ [16]. Studies have also shown that structural phase transition and superconductivity might be correlated in pure $IrTe_2$ [7,10,19–21]. This was because, in most previous experiments, it was found that upon substitution with transition metals such as Pd, Pt, Rh [7,8,19,20] or intercalation with Cu [21], the structural transition was suppressed and bulk superconductivity emerged with $T_c \sim 3$ K. The appearance of bulk superconductivity upon Pt substitution in such a large spin-orbit-coupled material may give rise to exotic states of matter such as topological superconductivity [22,23].

Recently, several transition metal dichalcogenides $PtTe_2$ [24], $PdTe_2$ [25,26], and $PtSe_2$ [27] were reported to host type-II Dirac fermions. The Dirac points in these transition-metal dichalcogenides (TMDs) lie far below E_F due to which the Dirac fermions have little contribution to the low-energy excitations near E_F. Angle-resolved photo emission spectroscopy (ARPES) experiments revealed that $IrTe_2$ is also a Dirac semimetal [28]. Due to the similar electronic structure of $IrTe_2$ and $PtTe_2$, in which the Dirac points lie above and below Fermi level (E_F), respectively, the Dirac point in $IrTe_2$ can be tuned to E_F by doping Pt at Ir sites while preserving the crystal structure holding the Dirac points. Doping with 10% Pt successfully tunes the Fermi level (E_F) to the Dirac point of the system. For this doping, as per ARPES experiments, two linearly dispersive bands cross each other at the Fermi level (E_F) thereby leading to a point-like Fermi surface (FS) at the Brillouin zone (BZ) center [29]. From band-structure calculations, it was argued that the Dirac point in $Ir_{1-x}Pt_xTe_2$ would fall at E_F for $x = 0.3$ [30]. This discrepancy between the ARPES experiment and the calculations was attributed to an inaccuracy in the calculations where the Dirac point energy was thought to be overestimated. The similar kind of inconsistency was also reported in $PtTe_2$ with a discrepancy of $\sim$ 0.1 eV between experiments and calculations [24].

Now we note that the Pt dopants not only make type-II Dirac fermions approach E_F, but also induce bulk supercon-

*goutam@iisermohali.ac.in

ductivity in the system. Certain experiments also showed that the Dirac point is relatively closer to the Fermi level in crystals displaying superconductivity [30]. In such cases, there is a possibility that the Dirac fermions take part in forming the superconducting condensate, thereby leading to topological superconductivity. It has been shown from ARPES experiments that there are mainly two bands α and β contributing to the FS which originate from the Te p_z orbital and the Te $(p_x + p_y)$ orbitals, respectively [31]. For the parent compound $IrTe_2$, it is shown that the structural transition is associated with a type-II van Hove singularity appearing in the β band. The β band dispersion preserves the corresponding saddle point below E_F in the systems with lower Pt doping samples, which show superconductivity [11]. To note, Yao and Yang proposed that a spin-triplet pairing instability may occur in 2D electron systems when the band filling is near a particular type of van Hove singularity (VHS), namely the type-II VHS [32]. In that context, the system under study may, in principle, also host p-wave superconductivity [33].

From the structural point of view, $IrTe_2$ exhibits an ordered state below the structural transition T_s and the existence of supermodulation (SM) with the wave vector $q = 2\pi/5a_m$ (a_m is the lattice constant in a monoclinic phase) was reported by scanning tunneling microscopy (STM) [34] and diffraction studies [3–5,7,12]. The STM studies at 80 K also revealed the coexistence of various incommensurate phases on the surface of $IrTe_2$. It was suggested that a partially opened pseudogap state associated with the coexisting structures gives rise to temperature- and energy-dependent electronic roughness on the surface. As the temperature is lowered, the system undergoes a structural phase transition from such incommensurate phases to the ground state with commensurate 1/6 structural modulation [13]. Whether the structural transition is related to a charge density wave (CDW) transition or not is still a matter of debate [7,13]. The emergence of superconductivity in doped $IrTe_2$ is related to disappearance of the ordered state. The evolution of SM with Pt doping and its effect on the structure and electronic states has been investigated in the past. Such studies on $Ir_{1-x}Pt_xTe_2$ by scanning tunneling microscopy and spectroscopy (STM/S) at 4.2 K have shown that low Pt concentration samples, which show the structural transition, exhibit SM with a fixed wave vector as in $IrTe_2$ while optimal Pt doping samples that exhibit superconductivity display a patchwork structure [35]. However, the correlation between the appearance of the patchwork structure and the nature of superconductivity still remains an open question. Therefore, it is necessary to investigate the superconducting phase of Pt-$IrTe_2$ in detail, particularly near a critical doping (10%) for which the Dirac point is expected near the E_F [29,31].

II. RESULTS AND DISCUSSION

In this paper, we report STM/S results on 10% Pt-doped $IrTe_2$. For the scanning tunneling microscopic and scanning tunneling spectroscopic measurements presented in this paper, we used high-quality single crystals of Pt-doped $IrTe_2$ with 10% Pt in the crystals. The single crystals of 10% Pt-doped $IrTe_2$ were grown by the self-flux method. The starting elements Ir powder (99.99%, Alfa Aesar), Pt powder (99.9%, Alfa Aesar), and Te shots (99.9999%, Alfa Aesar) were taken in the atomic ratio of $0.18(1-x) : 0.18x : 0.82$ and placed in an alumina crucible. Then the crucible was sealed in an evacuated quartz tube. In the first step, the quartz tube was heated to 950° C in 15 h and kept at this temperature for 10 h. The temperature was then increased to 1160° C in 20 h and maintained for 24 h. The melt was then slowly cooled down to 890° C at a rate of 2° C/h. At this temperature, excess Te was removed by a centrifuge.

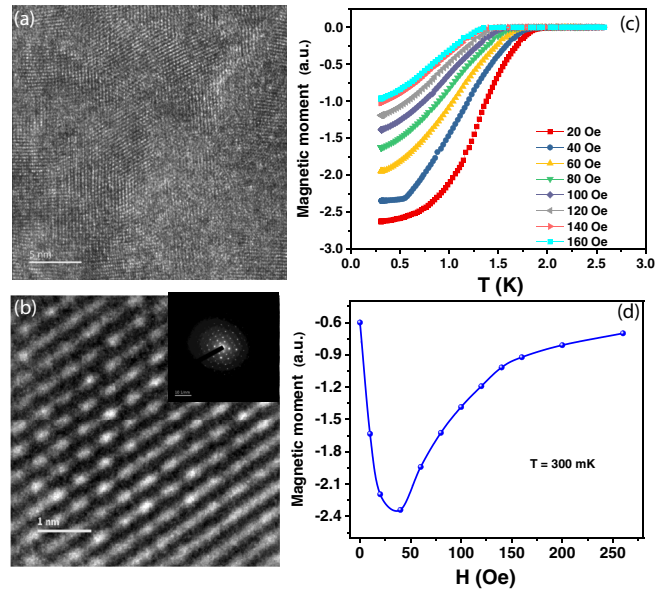

FIG. 1. (a) TEM image (30 nm × 30 nm) of the cleaved $Pt_{0.1}Ir_{0.9}Te_2$ surface. (b) Atomic resolution image under a transmission electron microscope (TEM) Inset: A selected area electron diffraction (SAED) pattern of the image shown in (b). (c) Magnetic moment versus temperature curve at different magnetic fields. (d) Magnetic moment as a function of applied field for $Ir_{0.9}Pt_{0.1}Te_2$ at 300 mK.

All the experiments presented in this paper were done using the ultrahigh vacuum cryostat working down to 310 mK (Unisoku system with RHK R9 controller). The shiny single crystals were first mounted in an ultrahigh vacuum (UHV) cleaving stage and the crystals were then cleaved at 80 K using an *in situ* cleaver. The contamination of the sample surface was minimized with this process. After cleaving, the crystals were immediately transferred to the STM head by a UHV manipulator which goes down to 310 mK using a He^3-based cryostat. The sample is placed at the center of a solenoidal superconducting magnet with a maximum field strength of 11 Tesla. All the STM/S measurements were done with sharp metallic tips of tungsten (W). STM images were obtained in constant-current mode. The tips were fabricated by electrochemical etching and were cleaned by electron-beam bombardment under UHV in a preparation chamber attached to the STM prior to the low-temperature experiments. The high quality of single crystals was confirmed by STM as well as by transmission electron microscopy (TEM). Figure 1(a) shows the low-magnification TEM image of Pt-$IrTe_2$, which reveals the layered arrangement along the crystallographic c-axis. The atomic resolution

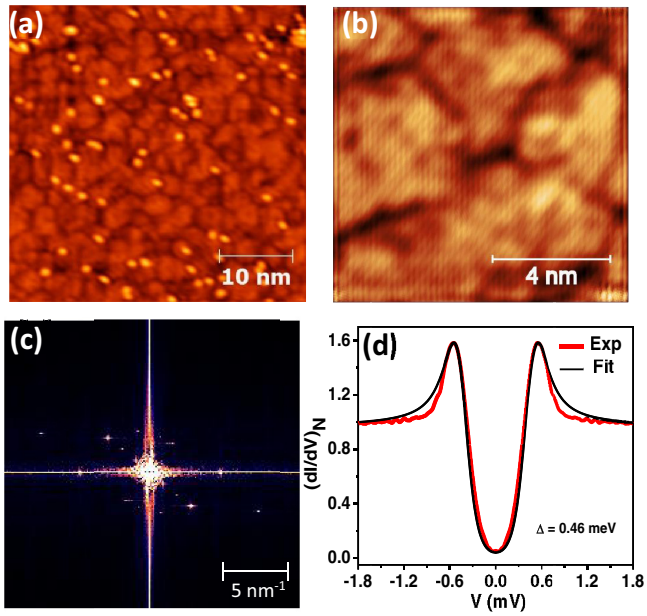

FIG. 2. (a) STM image (40 nm × 40 nm) of the cleaved Pt-$IrTe_2$ surface. (b) Zoomed image of the image in (a). (c) Fast Fourier transform (FFT) of the image shown in the main panel. (d) A representative scanning tunneling spectrum with the best theoretical fit at 310 mK (bias voltage = 3.6 mV; tunneling current (I) = 0.63 nA; lock in voltage = 0.1 mV).

imaging under a high-resolution transmission electron microscope (HRTEM) depicting the hexagonal atomic arrangement of Te atoms and the corresponding selected area electron diffraction (SAED) pattern is shown in Fig. 1(b) and the inset of Fig. 1(b), respectively. The bulk magnetization data show strong diamagnetism, indicating that our sample is superconducting with a critical temperature T_c of about 1.8 K at $H_{\text{ext}} = 20$ Oe. The superconducting transition temperature (T_c) decreases monotonically with the applied magnetic field, as shown in Fig. 1(c). In Fig. 1(d), we show the magnetic moment as a function of the applied field H_a at 300 mK. The $M(H_a)$ curve follow the typical behavior of a type-II superconductor, which is consistent with the STM data discussed later.

In Fig. 2(a) we show the STM image of the $Ir_{0.9}Pt_{0.1}Te_2$ surface captured at 320 mK. In this 40 nm × 40 nm area we can clearly see patches of few nm^2 area are formed. The size and direction of the patches is random. This peculiar structure was termed as a "patchwork structure (PS)" by Fujisawa *et al.* [35]. In addition to the patches, some bright clusters are also observed on the surface. These bright objects are the defect states possibly of Pt with which the system has been doped. They are randomly distributed all over the surface. If we look at the zoomed view [Fig. 2(b) of the image shown in Fig. 2(a), we observe several dark spots along with the patches on the surface of $Ir_{0.9}Pt_{0.1}Te_2$ as shown in Fig. 2(b). Such dark spots are the defects that might be due to the Te vacancies in the crystals. The origin of the PS is not clear. It was argued that the PS might be related to the reduction of structural stress due to the Pt dopant. The inhomogeneity can be seen in the STM images [Figs. 1(a) and 1(b)], and due to this background inhomogeneity, the amplitude of the gap and the corresponding critical temperature was also seen to vary at different points on the surface. A number of spectra obtained at randomly chosen points on the surface are shown in the Supplemental Materials (Fig. S3) [36]. We did not find any direct correlation between the amplitude of the gap with any special topographic feature. Figure 2(c) shows the fast Fourier transform (FFT) of the STM image shown in Fig. 2(b). We performed TEM imaging to understand the patchwork-like structure seen in the STM images. It is to be noted that the patchwork structure seen in the STM topography is not observed in the TEM images.

After confirming the pristine nature of the surface through atomic resolution imaging, we performed local scanning tunneling spectroscopy on the surface of Pt-$IrTe_2$. Figure 2(d) shows a representative scanning tunneling spectrum where coherence peaks symmetric about $V = 0$ can be clearly seen. A slight asymmetry was seen in the STM spectra. The presented data in this paper were symmetrized and smoothed by five point adjacent averaging to compare with the theoretically generated spectra. The position of these peaks provides an estimate of the superconducting energy gap (Δ) of a superconductor. At zero bias, the conductance is approximately zero. This spectrum is nicely fitted by the Dyne's equation given by $N_s(E) = \text{Re}(\frac{(E-i\Gamma)}{\sqrt{(E-i\Gamma)^2-\Delta^2}})$, where $N_s(E)$ is the density of states at energy E, Δ is the superconducting energy gap, and Γ is an effective broadening parameter incorporated to take care of the slight broadening of the Bardeen-Cooper-Schrieffer (BCS) density of states possibly due to a finite quasiparticle lifetime [37]. For the spectra shown in Fig. 2(d), the extracted value of Δ is 460 μeV at 310 mK.

To investigate the superconducting phase in Pt-$IrTe_2$, we carried out the temperature dependence of the dI/dV spectrum. The position of the coherence peaks do not show a significant change at low temperatures, indicating the gap is constant at low temperatures. The coherence peaks close smoothly with increasing temperature and all the spectral features disappear at a critical temperature of 1.75 K [Fig. 3(a)]. As shown by the dots in Fig. 3(b), Δ decreases smoothly to zero following $\Delta(T) \sim (1 - \frac{T}{T_c})^{1/2}$ near $T_c \sim 1.75$ K, as expected for a conventional BCS superconductor. The critical temperature thus measured is consistent with the value measured from transport data [30]. From the measured values of Δ_0 and T_c, Δ_0/K_BT_c is found to be ~ 3, which falls well within the limit of the strong coupling superconductor. While the $IrTe_2$ and lower Pt doping samples were found to lie in the BCS weak coupling limit [16,19,38], $Ir_{0.9}Pt_{0.1}Te_2$ falls in the strong coupling limit. Hence, at some point, there must be a crossover from weak coupling to strong coupling limit as the doping is increased. This might be associated with the enhancement in the density of states at the Fermi level with increasing doping concentration. It should be noted that, apart from the coherence peaks and smooth decay of the spectrum at higher temperatures, no other special spectral features are observed. This further indicates the absence of any unconventional component in the superconducting order parameter of Pt-$IrTe_2$, which is consistent with the previous reports [39–41]. The temperature dependence at two other different points is shown in Fig. S1 [36]. In both cases, the

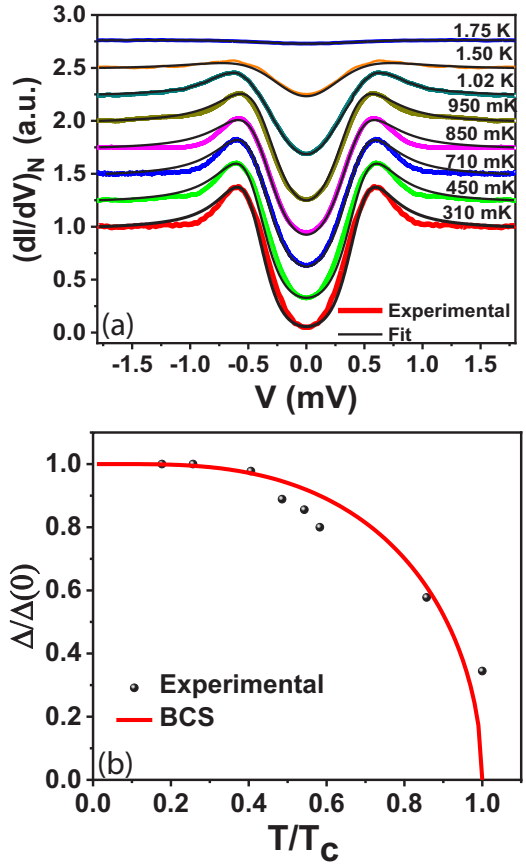

FIG. 3. (a) Normalized STS spectra at different temperatures from 310 mK to 1.75 K. Colored lines represent the experimental data points and solid lines show theoretical fits within BCS theory. (b) Δ versus T plot. Black dots show the values of Δ extracted from (a) while the red line shows the temperature dependence within BCS theory.

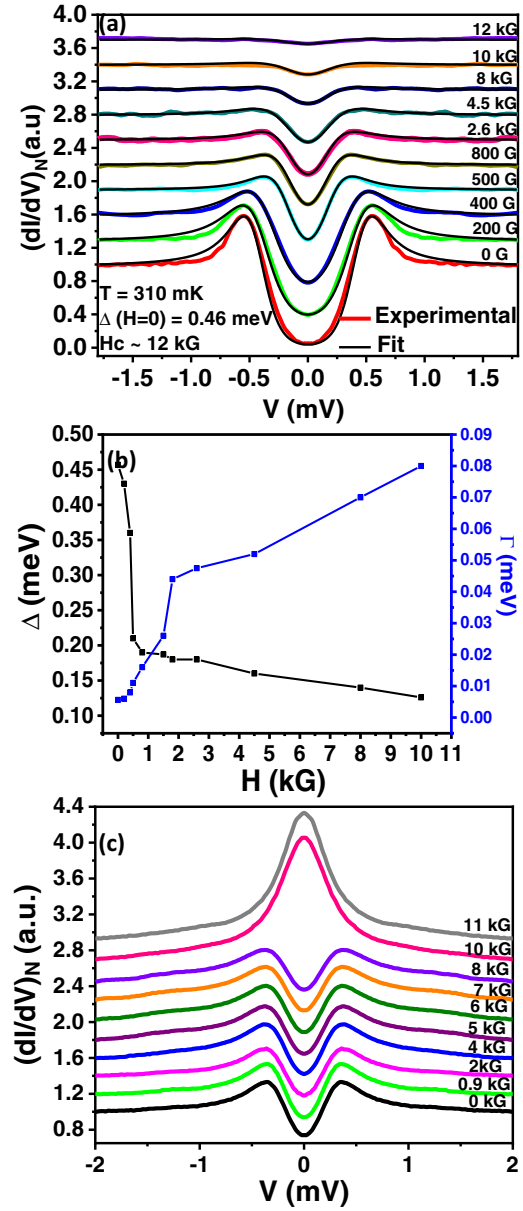

FIG. 4. (a) Normalized STS spectra at different magnetic fields from 0 kG to 12 kG at 310 mK. Colored lines represent the experimental data points and solid lines show theoretical fits within BCS theory. (b) Δ and Γ versus H plot. Black and blue dots show the values of Δ and Γ extracted from (a), respectively. (c) Spectra recorded in the presence of magnetic field showing zero bias peak at 10 kG.

critical temperature was observed to be different from that in Fig. 3 presented above. As we mentioned earlier, the variation might be related to the inhomogeneity seen in the STM topographic images. As it is seen in Fig. S1(b), we obtain one spectrum where the features differ from all other spectra and could not be described by Dyne's formula [36]. The origin of this is not understood, but the rarity of such features indicate that it might be related to some extrinsic factors (e.g., a strong local disorder).

Now we focus on the behavior of the superconducting phase as a function of increasing magnetic field (H). In Fig. 4(a), we show the evolution of the tunneling spectrum with magnetic field along with their Dyne's fit at 310 mK. The field is applied perpendicular to the *ab* plane of the crystal. The spectral features were seen to disappear continuously with increasing field, eventually vanishing at a field of 1.2 T. From this information, the coherence length was calculated to be 16 nm. The variation of Δ and Γ with increasing magnetic field is shown in Fig. 4(b) where a smooth disappearance of the gap is clearly visible. Another point to be noted here is a sudden change in the value of Δ at $H = 500$ G. At this field, Δ decreases to almost 50% of the zero-field value. In type-II superconductors, such a sudden change in Δ is attributed to the formation of vortices near the STM tip. At the same time, Γ gets almost doubled of its value at zero field. Γ represents a pair-breaking mechanism due to a finite lifetime, which is consistent with the field-induced pair breaking, possibly due to the formation of a vortex core. In our measurements, we also find spectra with a zero bias conductance peak when a magnetic field is applied [Fig. 4(c)]. This can be understood as the sudden appearance of a vortex under the STM tip. The magnetic field dependence at another point is shown in Fig. S2 where the smooth evolution of the superconducting energy gap upto 11 kG can be seen [36]. All these establish

$Ir_{0.9}Pt_{0.1}Te_2$ as a type-II superconductor. The variation in the detail of the features could be attributed to the relative distance of the points of measurements from the vortex cores possibly appearing on the surface [42,43].

III. CONCLUSION

In conclusion, we performed comprehensive studies on the superconducting phase of Pt-doped $IrTe_2$ at different temperatures and magnetic fields. Through our detailed scanning tunneling microscopic and spectroscopic measurements, we showed that $Ir_{0.9}Pt_{0.1}Te_2$ is a conventional BCS-like *s*-wave superconductor. Based on the calculated value of Δ_0/K_BT_c, our results show that $Ir_{0.9}Pt_{0.1}Te_2$ is a strongly coupled superconductor. Magnetic field-dependent studies also confirm that $Ir_{0.9}Pt_{0.1}Te_2$ is a type-II superconductor that can be clearly seen in the *M*-*H* data presented in Fig. 1(d). Here, we recall that a similar conventional superconducting phase was reported in the type-II Dirac semimetal $PdTe_2$ [44,45]. All such measurements collectively indicate that the mere coexistence of Dirac physics and superconductivity does not guarantee unconventional or topological superconductivity in solids.

ACKNOWLEDGMENTS

The authors would like to acknowledge Anshu Sirohi and Suman Kamboj for their help during various stages of this work. We acknowledge use of the SQUID magnetometer facility at IISER Mohali. A.V. thanks UGC for a senior research fellowship (SRF). D.R. thanks DST INSPIRE for financial support. G.S. thanks financial support from a research grant (Grant No. DST/SJF/PSA-01/2015-16) under a Swarnajayanti Fellowship awarded by the Department of Science and Technology, Government of India.

[1] C. S. Lee and G. J. Miller, Inorg. Chem. **38**, 5139 (1999).
[2] A. Kiswandhi, J. S. Brooks, H. B. Cao, J. Q. Yan, D. Mandrus, Z. Jiang, and H. D. Zhou, Phys. Rev. B **87**, 121107(R) (2013).
[3] H. Cao, B. C. Chakoumakos, X. Chen, J. Yan, M. A. McGuire, H. Yang, R. Custelcean, H. Zhou, D. J. Singh, and D. Mandrus, Phys. Rev. B **88**, 115122 (2013).
[4] G. L. Pascut, K. Haule, M. J. Gutmann, S. A. Barnett, A. Bombardi, S. Artyukhin, T. Birol, D. Vanderbilt, J. J. Yang, S.-W. Cheong, and V. Kiryukhin, Phys. Rev. Lett. **112**, 086402 (2014).
[5] T. Toriyama, M. Kobori, T. Konishi, Y. Ohta, K. Sugimoto, J. Kim, A. Fujiwara, S. Pyon, K. Kudo, and M. Nohara, J. Phys. Soc. Jpn. **83**, 033701 (2014).
[6] N. Matsumoto, K. Taniguchi, R. Endoh, H. Takano, and S. Nagata, J. Low Temp. Phys. **117**, 1129 (1999).
[7] J. J. Yang, Y. J. Choi, Y. S. Oh, A. Hogan, Y. Horibe, K. Kim, B. I. Min, and S.-W. Cheong, Phys. Rev. Lett. **108**, 116402 (2012).
[8] D. Ootsuki, Y. Wakisaka, S. Pyon, K. Kudo, M. Nohara, M. Arita, H. Anzai, H. Namatame, M. Taniguchi, N. L. Saini, and T. Mizokawa, Phys. Rev. B **86**, 014519 (2012).
[9] D. Ootsuki, S. Pyon, K. Kudo, M. Nohara, M. Horio, T. Yoshida, A. Fujimori, M. Arita, H. Anzai, H. Namatame, M. Taniguchi, N. L. Saini, and T. Mizokawa, J. Phys. Soc. Jpn. **82**, 093704 (2013).
[10] A. F. Fang, G. Xu, T. Dong, P. Zheng, and N. L. Wang, Sci. Rep. **3**, 1153 (2013).
[11] T. Qian, H. Miao, Z. J. Wang, X. Shi, Y. B. Huang, P. Zhang, N. Xu, L. K. Zeng, J. Z. Ma, P. Richard, M. Shi, G. Xu, X. Dai, Z. Fang, A. F. Fang, N. L. Wang, and H. Ding, New J. Phys. **16**, 123038 (2014).
[12] Y. S. Oh, J. J. Yang, Y. Horibe, and S. W. Cheong, Phys. Rev. Lett. **110**, 127209 (2013).
[13] Q. Li, W. Lin, J. Yan, X. Chen, A. G. Gianfrancesco, D. J. Singh, D. Mandrus, S. V. Kalinin, and M. Pan, Nat Commun. **5**, 5358 (2014)
[14] C. J. Raub, V. B. Compton, T. H. Geballe, B. T. Matthias, J. P. Maita, and G. W. Hull, J. Phys. Chem. Solids **26**, 2051 (1965).
[15] X. Zhang, J. Wang, Y. Liu, W. Zheng, and J. Wang, J. Phys. Chem. Solids **128**, 245 (2019).
[16] G. Cao, W. Xie, W. A Phelan, J. F. DiTusa, and R. Jin, Phys. Rev. B **95**, 035148 (2017).
[17] X. Li, J.-Q. Yan, D. J. Singh, J. B. Goodenough, and J.-S. Zhou, Phys. Rev. B **92**, 155118 (2015).
[18] S. Pyon, K. Kudo, and M. Nohara, Physica C: Superconductivity **494**, 80 (2013).
[19] S. Pyon, K. Kudo, and M. Nohara, J. Phys. Soc. Jpn. **81**, 053701 (2012).
[20] K. Kudo, M. Kobayashi, S. Pyon, and M. Nohara, J. Phys. Soc. Jpn. **82**, 085001 (2013).
[21] M. Kamitani, M. S. Bahramy, R. Arita, S. Seki, T. Arima, Y. Tokura, and S. Ishiwata, Phys. Rev. B **87**, 180501(R) (2013).
[22] A. P. Schnyder, S. Ryu, A. Furusaki, and A. W. W. Ludwig, Phys. Rev. B **78**, 195125 (2008).
[23] L. Fu and E. Berg, Phys. Rev. Lett. **105**, 097001 (2010).
[24] M. Yan, H Huang, K. Zhang, E. Wang, W. Yao, K. Deng, G. Wan, H. Zhang, M. Arita, H. Yang, Z. Sun, H. Yao, Y. Wu, and S. Fan, W. Duan, and S. Zhou, Nat. Commun. **8**, 257 (2017).
[25] F. Fei, X. Bo, R. Wang, B. Wu, J. Jiang, D. Fu, M. Gao, H. Zheng, Y. Chen, X. Wang, H. Bu, F. Song, and X. Wan, B. Wang, and G. Wang, Phys. Rev. B **96**, 041201(R) (2017).
[26] H.-J. Noh, J. Jeong, E.-J. Cho, K. Kim, and B. I. Min, and B.-G. Park, Phys. Rev. Lett. **119**, 016401 (2017).
[27] K. Zhang, M. Yan, H. Zhang, H. Huang, M Arita, Z. Sun, W. Duan, Y. Wu, and S. Zhou, Phys. Rev. B **96**, 125102 (2017).
[28] M. S. Bahramy, O. J. Clark, B.-J. Yang, J. Feng, L. Bawden, J. M. Riley, I. Markovic, F. Mazzola, V. Sunko, D. Biswas, S. P. Cooil, M. Jorge, J. W. Wells, M. Leandersson, T. Balasubramanian, J. Fujii, I. Vobornik, J. E. Rault, T. K. Kim, M. Hoesch, K. Okawa, M. Asakawa, T. Sasagawa, T. Eknapakul, W. Meevasana, and P. D. C. King, Nat. Mater. **17**, 21 (2018).
[29] B.-B. Fu, C.-J. Yi, Z.-J Wang, M. Yang, B.-Q Lv, X. Gao, M. Li, Y.-B. Huang, H.-M. Weng, Y.-G. Shi, T. Qian, and H. Ding, Chin. Phys. B **28**, 037103 (2019).

[30] F. Fei, X. Bo, P. Wang, J. Ying, J. Li, K. Chen, Q. Dai, B. Chen, Z. Sun, M. Zhang, F. Qu, Y. Zhang, Q. Wang, X. Wang, L. Cao, H. Bu, F. Song, X. Wan, and B. Wang, Adv. Mater. **30**, 1801556 (2018).

[31] J. Jiang, S. Lee, F. Fei, F. Song, E. Vescovo, K. Kaznatcheev, F. J. Walker, and C. H. Ahn, APL Mater. **8**, 061106 (2020).

[32] H. Yao and F. Yang, Phys. Rev. B **92**, 035132 (2015).

[33] Z. Y. Meng, F. Yang, K.-S. Chen, H. Yao, and H.-Y. Kee, Phys. Rev. B **91**, 184509 (2015).

[34] T. Machida, Y. Fujisawa, K. Igarashi, A. Kaneko, S. Ooi, T. Mochiku, M. Tachiki, K. Komori, K. Hirata, and H. Sakata, Phys. Rev. B **88**, 245125 (2013).

[35] Y. Fujisawa, T. Machida, K. Igarashi, A. Kaneko, T. Mochiku, S. Ooi, M. Tachiki, K. Komori, K. Hirata, and H. Sakata, J. Phys. Soc. Jpn. **84**, 043706 (2015).

[36] See Supplemental Material at http://link.aps.org/supplemental/10.1103/PhysRevB.105.094509 for more information on the spectra shown at randomly chosen points.

[37] R. C. Dynes, V. Narayanamurti, and J. P. Garno, Phys. Rev. Lett. **41**, 1509 (1978).

[38] M. N. Wilson, T. Medina, T. J. Munsie, S. C. Cheung, B. A. Frandsen, L. Liu, J. Yan, D. Mandrus, Y. J. Uemura, and G. M. Luke, Phys. Rev. B **94**, 184504 (2016).

[39] K. W.- Dong, M. Hu, Q. Tian, W. Z. Jun, X. Gang, F. A.- Fang, H. Y. Bo, Z. Peng, S. Xun, F. Zhong, D. Xi, R. Pierre, W. N. Lin, and D. Hong, Chin. Phys. Lett. **32**, 077402 (2015).

[40] S. Y. Zhou, X. L. Li, B. Y. Pan, X. Qiu, J. Pan, X. C. Hong, Z. Zhang, A. F. Fang, N. L. Wang, and S. Y. Li, Europhys. Lett. **104**, 27010 (2013).

[41] D. J. Yu, F. Yang, L. Miao, C. Q. Han, M.-Y. Yao, F. Zhu, Y. R. Song, K. F. Zhang, J. F. Ge, X. Yao, Z. Q. Zou, Z. J. Li, B. F. Gao, C. Liu, D. D. Guan, and C. L. Gao, D. Qian, and J.-F. Jia, Phys. Rev. B **89**, 100501(R) (2014).

[42] H. F. Hess, R. B. Robinson, R. C. Dynes, J. M. Valles, Jr., and J. V. Waszczak, Phys. Rev. Lett. **62**, 214 (1989).

[43] H. F. Hess, R. B. Robinson, and J. V. Waszczak, Phys. Rev. Lett. **64**, 2711 (1990).

[44] S. Das, Amit, A. Sirohi, L. Yadav, S. Gayen, Y. Singh, and G. Sheet, Phys. Rev. B **97**, 014523 (2018).

[45] Amit and Y. Singh, Phys. Rev. B **97**, 054515 (2018).